Friction https://mc03.manuscriptcentral.com/friction
https://doi.org/10.26599/FRICT.2026.9441223

Research Article

Enhancement of water lubrication in a rubber journal bearing by small-quantity oil

Tao Yu[1, 2], Feng Guo[1, 2 *], Hao Ji[1, 2], Xiaohan Zhang[1], Wenbin Duan[2], Peng Liang[1]

[1] *School of Mechanical & Automotive Engineering, Qingdao University of Technology, 777 Jialingjiang Road, Qingdao 266520, China*

[2] *Key Lab of Industrial Fluid Energy Conservation and Pollution Control of Ministry of Education, 777 Jialingjiang Road, Qingdao 266520, China*

* Corresponding author: Feng GUO, E-mail: mefguo@qut.edu.cn

Received: December 30, 2024; Revised: November 2, 2025; Accepted: January 26, 2026

Abstract: In this work, the idea of water lubrication enhanced by a small quantity of oil was tested for the first time in a rubber journal bearing. A small quantity of silicone oil was supplied to an eight-groove rubber bearing through a small nozzle, aiming to improve the lubrication of the bearings under short-time severe working conditions. Results demonstrated that the addition of small-quantity silicon oil can significantly reduce friction, with the coefficient of friction (COF) at certain speeds being lower than that achieved with either pure water or pure oil. If the oil was given under frequent and small-quantity supply, smaller time interval of oil supply has little impact on friction reduction.

Moreover, a simple method based on the Stribeck curve was proposed to roughly predict the COF reduction of water-lubricated journal bearings with small-quantity oil supply at low speeds. Additionally, computational fluid dynamics (CFD) simulations provided insights into the migration/diffusion of injected oil within the bearing, revealing a correlation between oil side leakage and COF.

Keywords: water-lubricated bearing; two-phase flow; CFD simulation; secondary lubricant

1 Introduction

Water-lubricated stern bearings (WLBs), fully submerged in water, offer both eco-friendliness and cost-effectiveness. Research on these bearings date back to the Industrial Revolution. WLBs in ships mainly consist of two parts: the shaft and the bushing. Given the function of the bushing in the system, it is primarily achieved through design of the bushing to improve the lubrication performance of WLBs. Nowadays the materials of water-lubricated bushings in ships are mainly non-metallic, such as wood [1,2], rubber [3–5], polymers [6,7], and reinforced polymer composites [8–11]. Lignum vitae have been decimated used in WLBs by over-logging and unsatisfactory tribological properties. Recently Guo et al. [12] refocus on the lignum vitae wood-derived composites for better lubricating performance. Rubber and polymer materials such as polytetrafluoroethylene (PTFE), polyamide (PA), polyurethane (PU), polyetheretherketone (PEEK) are used in WLBs with a tendency to use two or more materials to form composite materials. Yan [13] studied on tribological and vibration performance of a new UHMWPE/graphite/NBR material under different working conditions. The results indicated that the mechanical physical performance of the compound rubber material had reached the requirements of Chinese ship standard CB/T769-2008. Other materials such as ceramics [14] and two-dimensional (2D) material [15] have also provided insights for the development of low-friction WLBs. Advancements in materials have focused on friction and wear resistance, durability enhancement, environmental impact reduction, and performance under various operating conditions. Dedicated designs in bushing structures - including groove number [16] and its shape [17–19], liner design [20], and various microstructures [21–23] etc. have contributed to the durability of bearings. The structures of WLBs grooves are mainly divided into longitudinal grooves, spiral grooves [24] and herringbone grooves [25]. Longitudinal grooves are widely used due to their simple structure and good sand discharge, and when the number of grooves increases to 6-8 a stable hydrodynamic lubrication zone can be formed by balancing the water film [26]. Spiral grooves [27] have good mud and impurity discharge capacity. Herringbone grooves [28] can significantly improve bearing capacity. Multi-layered bushings [29] combine the advantages of various materials, such as a rubber layer for vibration absorption and a plastic layer for high wear resistance. Additionally extensive researches about fluid dynamics on water-lubricated bearings have been conducted to guide the design of WLBs [30–32]. Despite the above advancements of WLBs, there are challenges when the WLBs face harsh conditions like low speeds at start-up/shut-down, sudden impact or heavy loads, leading to water film collapse, increased friction, wear and noise, which reduce the lifespan of the bearings. Tackling these tribological issues remains a key focus in WLBs research [33]. Therefore, research on harsh operating conditions has become one of the keys focuses of WLBs.

Ouyang et al. [34] investigated the lubrication and vibration characteristics of water-lubricated stern bearing for underwater vehicles under harsh working conditions. The results showed that the polymer bearing was subjected to hydrolysis because of the increased heat generation and heat dissipation deterioration under low speed, heavy pressure, and high water temperature. Li et al. [35] elucidated the mechanism of wave impact on the dynamic bearing characteristics of ship shaft systems. Zhang [36] established the transient mixed lubrication model coupled with dynamic equation during start-stop cycle and reveals the transient asperity contacts and dynamic behaviors under different radial clearances and acceleration times. Some researches are also carried out towards other directions trying to solve the problem of low water load-carrying capacity. Wang [37] et al. proposed a magnetic-water double suspension elastic-supported thrust bearing, which utilizes both water film and permanent magnetic force to reduce solid contact. Li [38] et al. attempt to regulate the COF by changing the elastic modulus of rubber bearings through a magnetic field. Through the magnetic field [39] during operations the lubricant viscosity can be locally controlled, thus ensuring the presence of a lubricating film at critical operating conditions when boundary or mixed lubrication is normally expected. Xiong et al. [40] designed microcapsules with the oil core embedded in a resin matrix, where the capsules ruptured during the friction and wear process, releasing oil to enhance lubrication with the advantages of effective lubrication, environmental friendliness, and low cost. Zhang et al. [41] found that the trace oil released from the microcapsules at the sliding interface favored the formation of a hydrodynamic film and a boundary tribo-film with an ultralow shear strength. This work provided a novel method to achieve superlubricity with polymer composites. Yang et al. [42,43] have also introduced ionic liquids into microcapsules. However the microcapsules improving the lubricating properties of the materials is at the expense of mechanical properties [44].

Recently a new idea of actively supplying a small quantity of secondary lubricating medium to assist water lubrication was proposed by Guo and his co-workers [45,46] et al. With a block-on-ring test rig, they found that a small quantity of oil can significantly generate reductions in friction and wear under water lubrication, and the reduced friction could last for a pretty long time. This idea has a relatively smaller impact on the mechanical properties of bearings compared to microcapsules. However, the coefficient of friction (hereafter "COF") increased when the ring rotational speed exceeded the critical speed. Liang [47] et al. numerically calculated the oil diffusion behavior in a short period of time after a small quantity of oil supply for a water lubricated smooth journal bearing. In engineering practices, grooves of bearings play a role of heat dissipation and impurity removal.

Whether a small quantity of oil has an important impact on the water-lubricated journal bearings has not yet been studied.

This paper carried out tests and computational fluid dynamics (CFD) simulations to investigate the tribological characteristics of an eight-groove journal bearings with a small quantity of silicon oil as a secondary lubricant, and to clarify the silicon oil lubrication under water environment.

2 Operating conditions

2.1 Test bench and tribo-pairs

The water-lubricated bearing bench consists of an NBR bush with eight longitudinal grooves and a 316 stainless steel shaft, which are commonly used in ship propulsion systems. In the tests, the tribo-pair was submerged into water in a sealed chamber. The bush is floating and the shaft is fixed. Geometric parameters of the bush and the shaft are listed in Table 1. The radial clearance is 0.6 mm, which meets the permissible clearance value for water-lubricated bearings in practical applications. The load is applied to the bearing by a hydraulic unit. The shaft rotation is driven by an AC motor, and a torque sensor is used to measure the friction torque of the tribo-pair, as shown in Fig. 1(a). The oil supply nozzle is located in the entrance area, aligning with the direction of the horizontal radius of the bush, as illustrated in Fig. 1(b).

Table 1 Parameters of the tribo-pair.

	Materials	Surface roughness (Ra/μm)	Radius (mm)	Width (mm)	Oil nozzle (mm)	Grooves (mm)
Shaft	Stainless steel 316	0.8	R_1=50	336	-	-
Bush	NBR3606	0.8	R_2=50.6	80	Φ_3=10	R_4=1.5

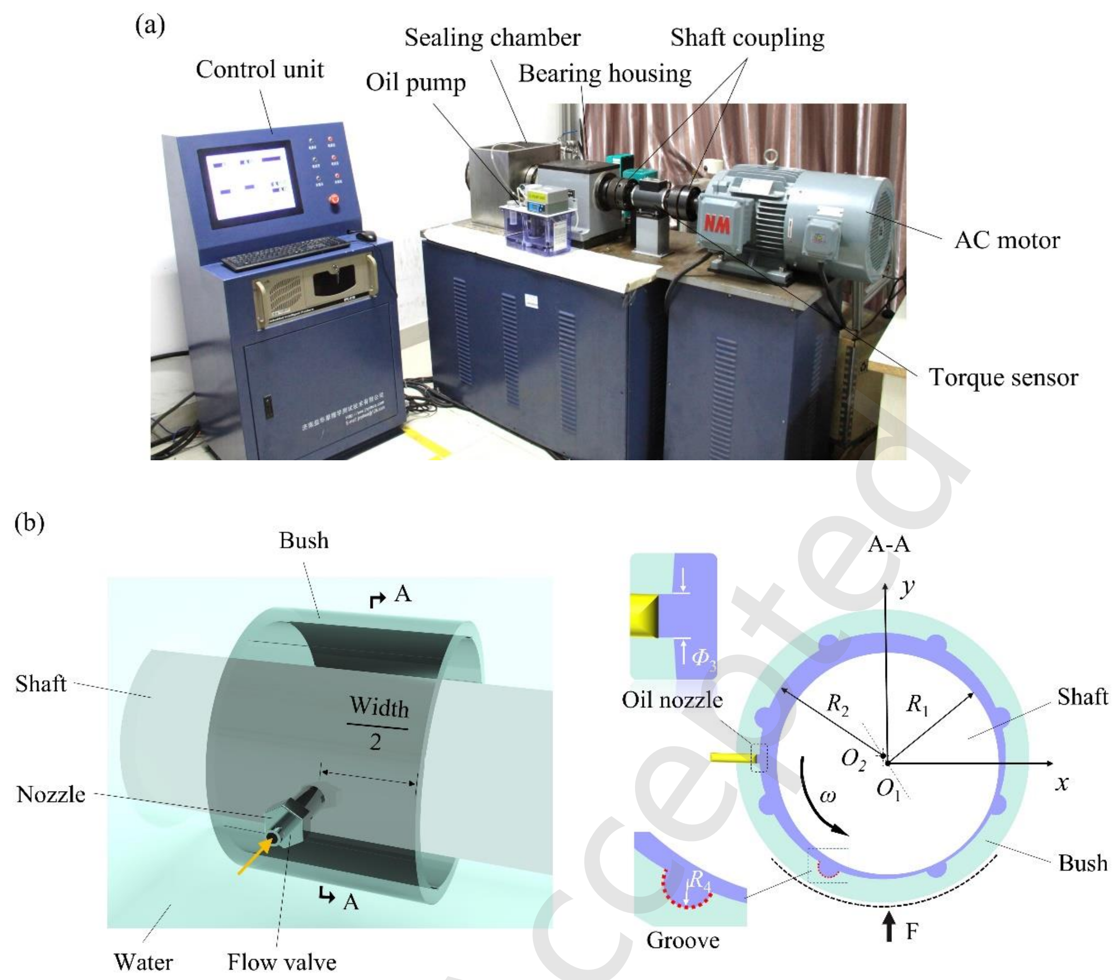

Fig. 1 (a) Water-lubricated bearing test bench; (b) schematic diagram of the tribo-pair.

2.2 Lubricants

The inlet water's temperature is 20±1℃ and its viscosity is 0.000955 Pa·s. Silicone oil is used as a secondary lubricant because of its low surface tension. The viscosity of silicone oil is 0.428 Pa·s, which is higher than the viscosity of the oil commonly used for stern tube bearings in order to significantly enhance the load-carrying capacity. The properties of the lubricants are listed in Table 2.

Table 2 Properties of lubricants.

Lubricants	Viscosity (Pa·s)	Density (kg/m^3)	Oil supply	Temperature
Water	0.000955	998.2	-	20℃
Silicone oil	0.4278	963	500 μL/s，4 s	

2.3 Test methods

In the bench tests, loads were applied to the bearings submerged underwater, and stepped shaft rotational speeds were employed for the purpose of running-in. Subsequently, friction tests at various rotational speeds and loads with pure water lubrication were carried out with a duration of 2 minutes for each test. Curves of COF vs. speed were obtained under various specific pressure, facilitating the identification of the lubrication regime. The specific pressure range was 0.063-0.5 MPa. The same scheme was also applied to measure the COF curve for pure silicone oil. However the oil level was at the lower 1/3 of the bearing height to reduce heat churning, and the results are presented in Fig. 2(b). As shown in Fig.2(a), under pure water lubrication the COF is higher at lower speeds and decreases with increasing speeds. Moreover, higher loads present lower COFs. From Fig. 2(a) it is easy to see that at the shaft speeds below 400 r/min the tribo-pair is in the regime of mixed lubrication, and boundary lubrication may be achieved at speed below 200 r/min under 0.5 MPa specific pressure. Therefore shaft speeds of 100 r/min, 200 r/min and 300 r/min were chosen for the experiments of oil-assisted water lubrication. Under pure silicone oil lubrication in Fig. 2(b), the COF increases gradually with increasing shaft rotational speed, and the lubrication regime is full film lubrication.

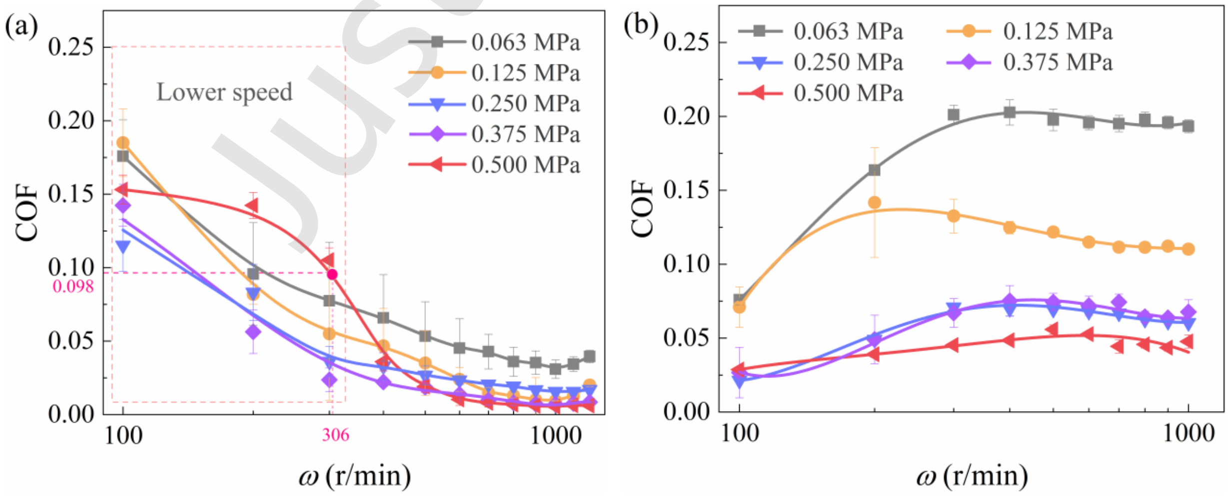

Fig. 2 COF vs. shaft speed under various specific pressures for (a) pure water and (b) silicone oil.

In the oil-assisted water lubrication test, the bearing was submerged in water and ran under a fixed specific pressure and a shaft rotational speed. Before oil is injected, the running-in is carried out under pure water lubrication. After the COF stabilized, a small quantity of silicone oil was supplied to the bearing. The oil supply rate is 500 μL/s and the supply time is 4 s, the total amount of oil is 2 mL. As an example, Fig. 3 shows that the COF can decrease significantly after a small quantity of oil is supplied to the bearing under water lubrication. Considering the time cost and to ensure the uniformity under different experimental conditions, the 4 min before oil supply and the 5 min after oil supply are taken for display. The data from 120 s to 240 s reached basic stability, so it is selected to calculate the average value of the COF under pure water lubrication. The data from 360 s to 540 s is used to calculate the average value of the COF after oil supply for the same reason. The oil-assisted water lubrication test was repeated twice under the same conditions. Before and after the tests, the tribo-pair was meticulously cleaned with petroleum ether and anhydrous ethanol.

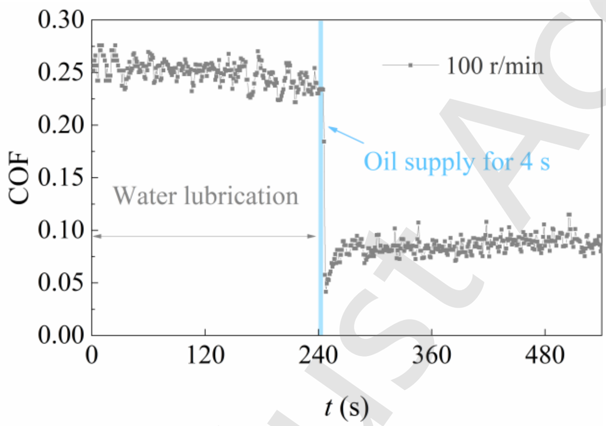

Fig. 3 COF vs. time (P = 0.05 MPa, ω = 100 r/min).

2.4 CFD simulation

The present study also employed computational fluid dynamics (CFD, ANSYS Fluent) to gain some insights into the oil transportation/diffusion after oil injected into the bearings. As shown in Fig. 4(a), in the calculation the radius clearance C_0 = 0.6 mm, the position angular Ψ =30°, the eccentricity e = 0.4 mm, and the eccentricity ratio is $\varepsilon = e/C_0$ = 0.67. The location on the circumference of the minimum film thickness ($h_{\min}$) is shown in Fig.4(a). Eight grooves are numbered as Groove 1 to Groove 8, as shown in Fig. 4(a). For the whole calculation domain hexahedral elements were used to reduce pseudo-diffusion at the phase interface. The Reynolds numbers (Re) for the rotational speeds (100 r/min, 200 r/min, and 300 r/min) are 52, 104 and 157, respectively, which are lower than the critical Reynolds number (1000), so a laminar flow model was chosen. The VOF model was used to calculate water-oil two phase flow, and a geometric reconstruction method is utilized to capture the phase interface. A continuous surface tension model (CSF) was implemented with an interface tension coefficient of 0.042 mN/m between silicone oil and water. The contact angles between silicone oil and solid surfaces underwater were measured to calculate wall adhesion, as illustrated in Figs. 4(c), (d), and (e). The diameter of the oil supply nozzle was 10 mm, and the oil supply adopted a velocity inlet of 0.04 m/s. At both end sides of the bush, pressure outlets were set at the atmospheric pressure. The PISO pressure-velocity coupling algorithm was employed to solve the momentum equations. Thermal effects were not considered at this time. Gradient interpolation based on the element-based least squares method was implemented for the diffusion term, and the PRESTO! scheme was used to calculate pressure values between two elements based on the element values in the discretization of the momentum equation, and a second-order upwind scheme was applied for the convection term.

Grid independence verification was performed in the calculations. The oil volume fractions at 0.48 s at the central cross section of the bearing were calculated under different grid numbers. Results show that the oil volume fraction with a grid number of 298,972 or more is similar, as shown in Fig. 4(f). Thus, the grid number of 298,972 was used for calculations. The calculation was started with pure water lubrication for 1 s, and then oil is supplied for 4 s, and the calculation was stopped until oil leakage is finished.

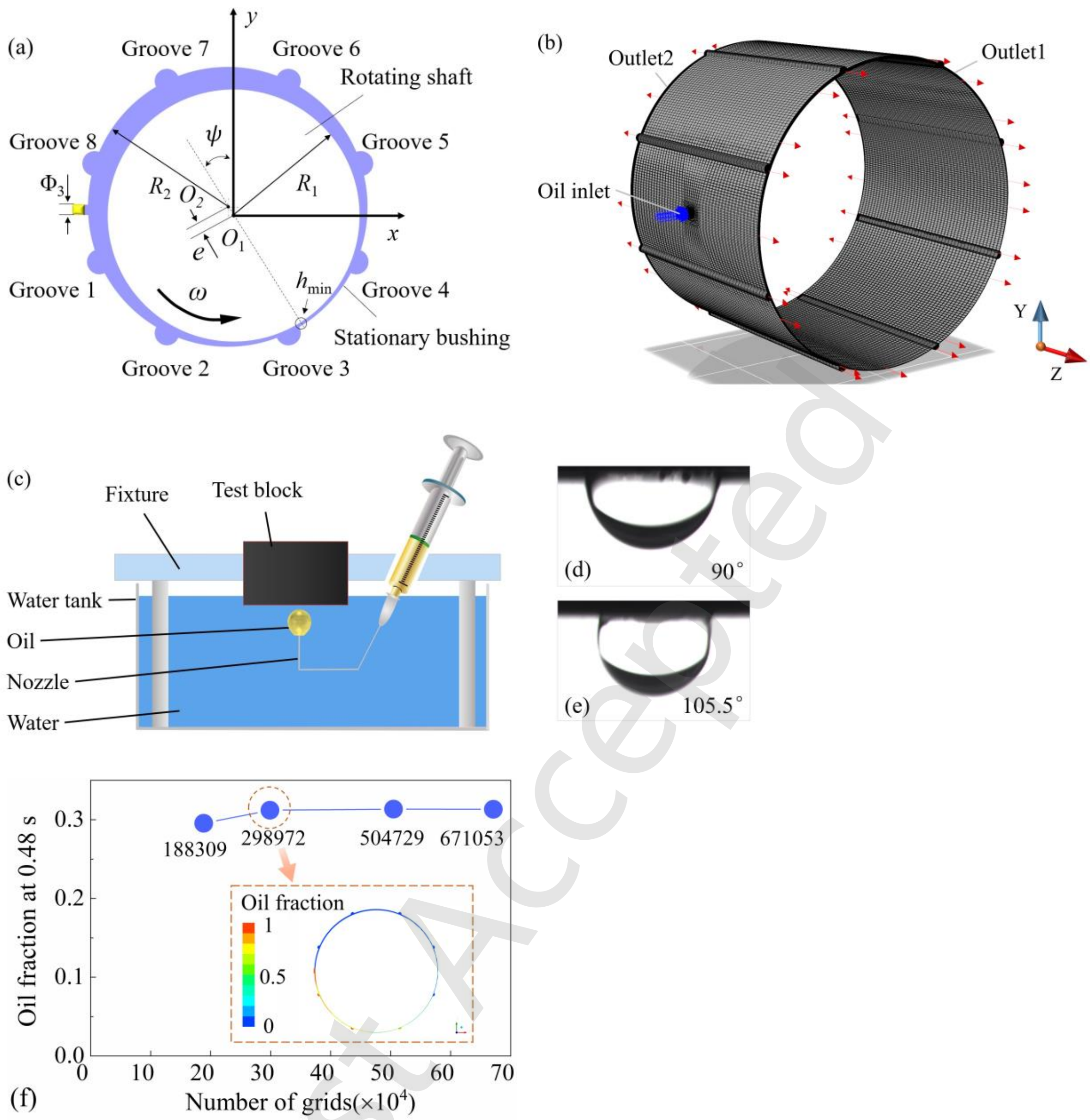

Fig. 4 (a) Schematic of the geometric model; (b) mesh grids; (c) setup of contact angle measurement underwater; (d) contact angle of silicone oil on NBR surface underwater; (e) contact angle of silicone oil on stainless steel surface underwater; (f) grid independence verification.

3 Results and discussions

3.1 Friction reduction with oil supply

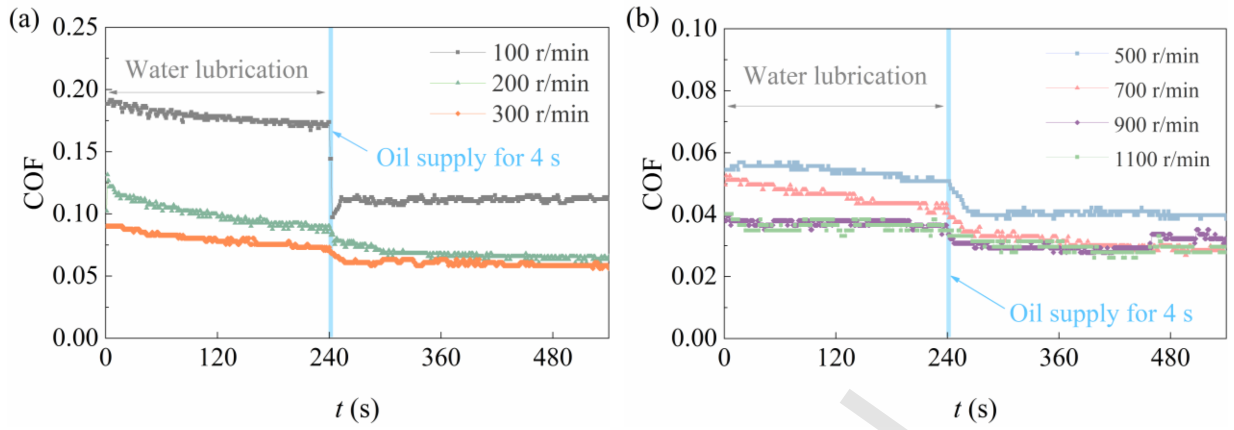

Fig. 5 COF vs. time under various shaft rotational speeds (P = 0.063 MPa): (a) At low speeds; (b) at high speeds.

Figure 5 depicts some of the results to illustrate the role of the silicone oil in assisting water lubrication as a second lubricating medium. 2 mL silicone oil (time = 4 s) is supplied into the clearance of the bearing at various shaft rotational speeds under a specific pressure of 0.063 MPa, and it can be seen that all the COFs show decrease after oil is injected. In particular, more obvious friction drop can be obtained at lower speeds, as shown in Fig. 5(a).

A COF reduction ratio, R_c, is denoted as:

$$R_c = (\mathrm{COF_{Water}} - \mathrm{COF_{LA}})/\mathrm{COF_{Water}} \times 100\% \quad (1)$$

where $\mathrm{COF_{Water}}$ is COF in pure water lubrication (taking the data from 120 s to 240 s), $\mathrm{COF_{LA}}$ is the COF after silicone oil is supplied underwater (taking the data from 360 s to 540 s).

At a shaft speed of 100 r/min, the COF rapidly drops from 0.17 to 0.11 after oil supply and R_c is 35.3%. Similarly at the shaft speeds of 200 r/min and 300 r/min, the COFs drop by 29.3% and 21.4%, respectively, remaining stable at the end of each test. When the injected oil enters the bearing the apparent viscosity of the lubricant increase, and consequently the load supported by liquid film increases, and that by solid contact decreases, which causes the COF to decrease. This friction reduction can also be described by the increase of the Hersey number (= $\eta v/P$) in the Stribeck curve as shown in Fig. 6. With pure water the bearing is under mixed lubrication, and its lubrication regime is represented by point A. With oil injected, the Hersey number increase to point B with increasing apparent viscosity, and consequently the friction decreases. At higher speeds, the COF reduction is low. In Fig. 2(a), it is easy to find that with increasing speed the COF curve reaches its valley region, where the contact is leaving the mixed lubrication regime. In this valley region, COF change is smaller than that in the region of mixed lubrication if similar Hersey number change is generated by the injection of a small quantity of oil, as shown in Fig. 6.

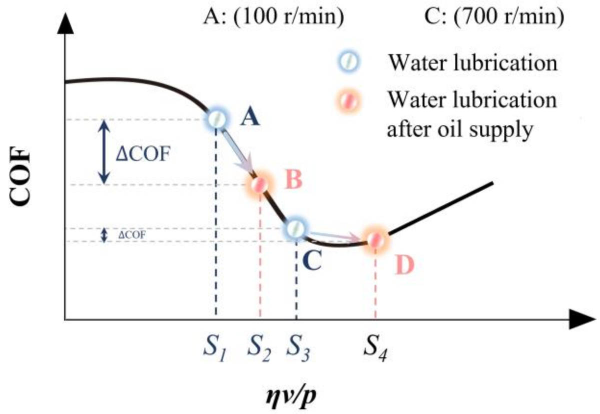

Fig. 6 COF change in water lubrication with a second lubricant in small quantity.

As stated above the present lubrication assistance by second lubricating medium is for short-time tough working conditions where the bearing is under boundary or mixed lubrication, therefore the tests were mainly conducted at higher specific pressures (0.125-0.5 MPa) and lower speeds (100-300 r/min). In Fig. 7, it can be seen that after a supply of small quantity silicone oil the COF is significantly reduced, and the low COF lasts until the end of the tests, which is similar to the test results under 0.063 MPa. It is well known that in the mixed lubrication regime of the Stribeck curve, lower pressure, higher speed and larger lubricant viscosity all lead to an increase in the Hersey number and a decrease in the COF.

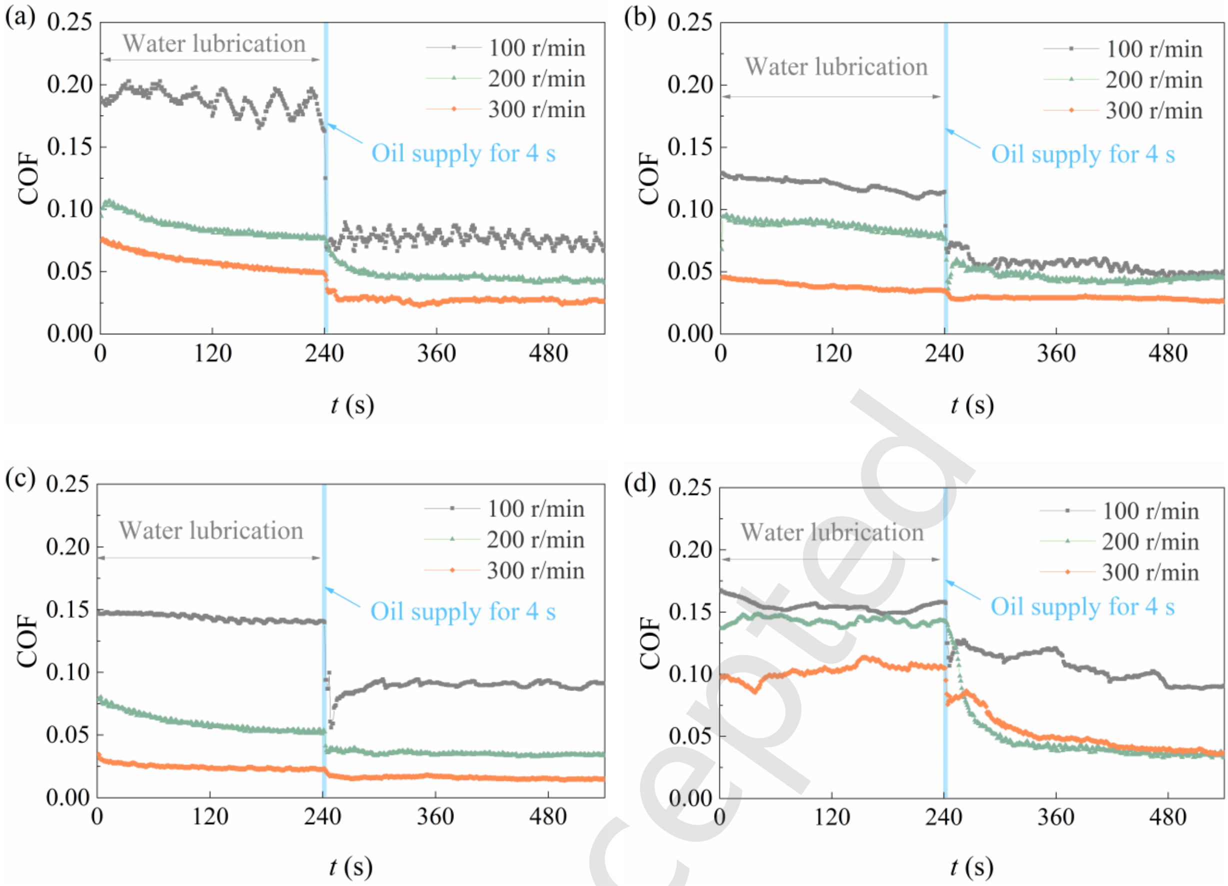

Fig. 7 COF vs. time under various pressures: (a) P = 0.125 MPa; (b) P =0.25 MPa; (c) P =0.375 MPa; (d) P =0.5 MPa.

The COF of pure silicone oil lubrication (denoted as $\mathrm{COF_{Oil}}$) was also measured, as shown in Fig. 2(b). It is found that the $\mathrm{COF_{LA}}$ may be lower than both $\mathrm{COF_{Water}}$ and $\mathrm{COF_{Oil}}$ under some working conditions, particularly at higher shaft speeds, as shown in Fig. 8. In the Stribeck curve, this means that the change in the apparent viscosity of the lubricant leads to the Hersey number to a position where the COF is lower. In addition, wear debris could be observed on the water surface during pure water lubrication tests. After oil supply, the wear debris is reduced but still exists. The wear debris suggests that hydrodynamic lubrication has not been fully achieved after oil supply.

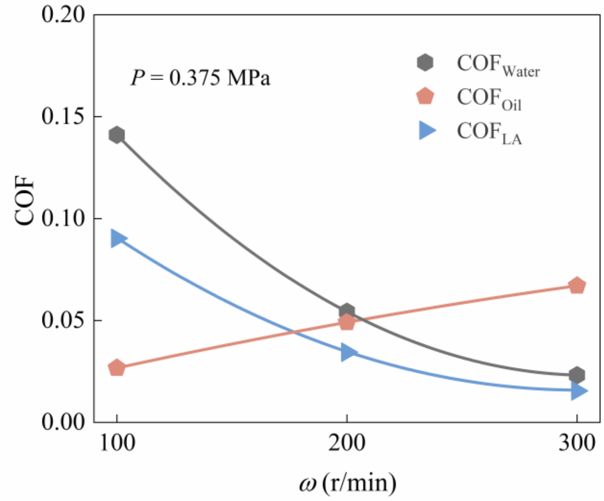

Fig.8 COF with three lubricants.

In the Stribeck curve, normally the same Hersey number present the same COF. Two different speeds, ω_{test} and ω_x, can give the same COF if two viscosities, η_{LA} and η_{water}, satisfies the follows,

$$\eta_{LA}\omega_{test} = \eta_{water}\,\omega_x \tag{2}$$

Where η_{water} is the is the viscosity of water (assumed to be constant at different speeds), η_{LA} is the apparent viscosity of the oil/water mixture in bearing clearance after oil supplied, ω_{test} is the experimental speed for oil-assisted lubrication in water, and ω_x is a pure water lubrication speed.

In the present experiments, after a small quantity of oil is supplied at speed of ω_{test}, the coefficient of friction decreases from COF_{water} to COF_{LA}, which is shown as point G to point H in Fig. 9. At point H, the corresponding speed ω_x can be known through the Stribeck curve or similar curves derived from the Stribeck curve, such as Fig. 2(a). Then η_{LA} can be known from Eq. (2). Assuming that the value of η_{LA} is considered a same constant at various speeds under the same load, the ω_x at different ω_{test} speeds can be calculated and its corresponding COF_{LA} can be predicted through the Stribeck curve or similar curves derived from the Stribeck curve under a certain load. For example, under ω_{test} = 100 r/min and P = 0.5 MPa in Fig. 7(d) COF_{LA} of 0.098 is gotten, and consequently the corresponding speed ω_x of 306 r/min can be found from the experimental data in Fig. 2(a), and apparent viscosity η_{LA} of 2.92 mPa·s is calculated by Eq. (2). It is easy to predict the corresponding ω_x for any other speed ω_{test}, and each corresponding COF_{LA} and R_c can be obtained.

The experimental R_c and predicted R_c are shown in Table 3. The predicted values of R_c under each load were calculated using the apparent viscosity η_{LA} at 100 r/min. At 0.5 MPa, the R_c errors of the predictions at various speeds are all less than 10%. At lower loads, the predicted values of R_c tend to be higher than those of the experiments and the prediction errors may larger than 10%, but no more than 25%. In fact, the above calculation only relies on the curve of COF vs. speed under pure water lubrication, as shown in Fig.2 (a).

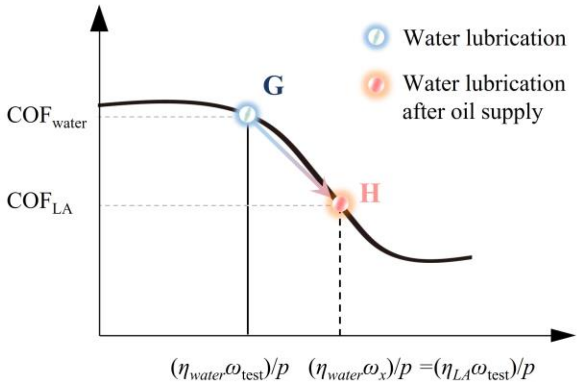

Fig. 9 Schematic diagram of Stribeck curve.

Table 3 COF reduction ratio R_c (%).

	Speeds	Experimental R_c (%)	Predicted R_c (%) (by η_{LA} at100 r/min)	ΔR_c (%)
0.5 MPa	100 r/min	36.1	36.1	0.0
	200 r/min	73.8	68.3	5.5
	300 r/min	61.0	67.3	6.3
0.375 MPa	100 r/min	36.0	36.0	0.0
	200 r/min	36.6	39.2	2.6
	300 r/min	33.3	24.9	8.4
0.25 MPa	100 r/min	54.6	54.6	0.0
	200 r/min	47.5	67.5	20
	300 r/min	21.1	43.8	22.7

0.125 MPa	100 r/min	58.4	58.4	0.0
	200 r/min	44.8	49.8	5.0
	300 r/min	48.7	67.6	18.9
0.063 MPa	100 r/min	35.3	35.3	0.0
	200 r/min	29.3	24.3	5
	300 r/min	21.4	33.9	12.5
	500 r/min	23.1	33.4	10.3

3.2 Friction fluctuations

To compare the fluctuation of bearing friction force (N) before and after oil supply, the standard deviation of friction force σ is calculated.

$$\sigma = \sqrt{\frac{\sum_{i=1}^{n}\left(F_{\mathrm{i}}-\bar{F}\right)^2}{n}} \quad (3)$$

Where F_{i} is the friction force (N) at time instant i, $\bar{F}$ is the average friction force (N), and n is the number of friction force data captured. The results of 100-300 r/min in Fig. 5 and Fig. 7 are used to calculate the σ of pure water lubrication and that after oil supply (taking the data from 120 s to 240 s or from 360 s to 540 s), as shown in Fig. 10.

Results show that σ after oil supply is similar to those of pure water lubrication under most conditions. At each speed in Fig. 10, σ shows an overall increase trend as the specific pressure increases. However, when a specific pressure of 0.5 MPa is reached, σ becomes larger after oil supply than that under pure water lubrication, which is correlated to Fig. 7(d). At high load, the greater pressure gradient presents greater resistance to oil entering the contact zone. When the actual supply of oil is unstable, it may cause a higher σ.

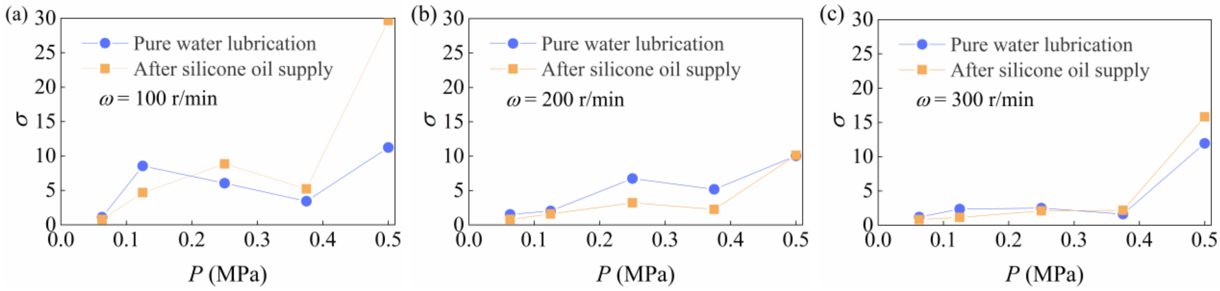

Fig. 10 σ before and after oil supply under various shaft rotational speeds.

3.3 Oil migration

It is of importance to understand the transportation/diffusion of the injected oil in the water-lubricated journal bearing. At present, it is not yet known in what state a small amount of oil is delivered to the bearings, and numerical simulation may be an easy approach to get some insight into this uncovered event. As has been observed, it takes some time for the COF to be stable after oil supply, which may be generated by the unsteady transportation of supplied oil within the bearing. In order to elucidate the migration of oil within the bearing underwater, CFD simulations have been carried out. The start time of oil injection is defined as t = 0 s. Fig. 11 shows the time instant t = 0.26 s at which the injected oil firstly arrives at the position of the minimum film thickness or get through load-bearing area on the shaft surface (denoted as t_1 = 0.26 s). The oil is dragged to the contact area mainly by the shaft surface after it is injected. Obviously, t_1 is evidently influenced by parameters such as the position of the oil supply nozzle, the shaft speed and the grooves etc. It is noted that the time is 0.15 s for the shaft to rotate from groove 1 to groove 3 and t_1 is much larger, which is attributed to the influence of the groove and inverse flow. As shown in Figs. 11(a) and 11(b), the oil/oil-water mixture on the surfaces of the shaft and the bush stays in the form of a strip along the circumferential center line because the side leakage/diffusion does not occur in such a short time. It is also interesting to find that the oil/oil mixture is discontinuous, which may be due to the lower wettability of oil on the two surfaces underwater. In the middle layer of the film the oil fraction is high near the nozzle, and then it becomes small when flowing into the bearing due to diffusion. After groove 2, the oil or oil-water mixture flow is disrupted and discrete oil/oil-water mixture appears. Fig.

11(c) shows the oil fraction at the A-A/central cross section of the bearing. It is natural oil fraction is larger near the nozzle. The oil fraction at the position of the minimum film thickness is also higher. Near the nozzle oil is supplied and accumulated due to its delayed transportation by the convergency gap and pressure gradient, therefore there is larger oil fraction and only a little oil further enters the convergent bearing gap. In the region between groove 1 and groove 2 and some part beyond groove 2, oil fraction is low. Anyway near groove 3 where gap decreases, the oil fraction increases again. Around groove 3 where pressure is built, there is side leakage by the pressure drop and more water is driven due to its low viscosity, which has contributed to the higher oil volume fraction near the minimum film thickness.

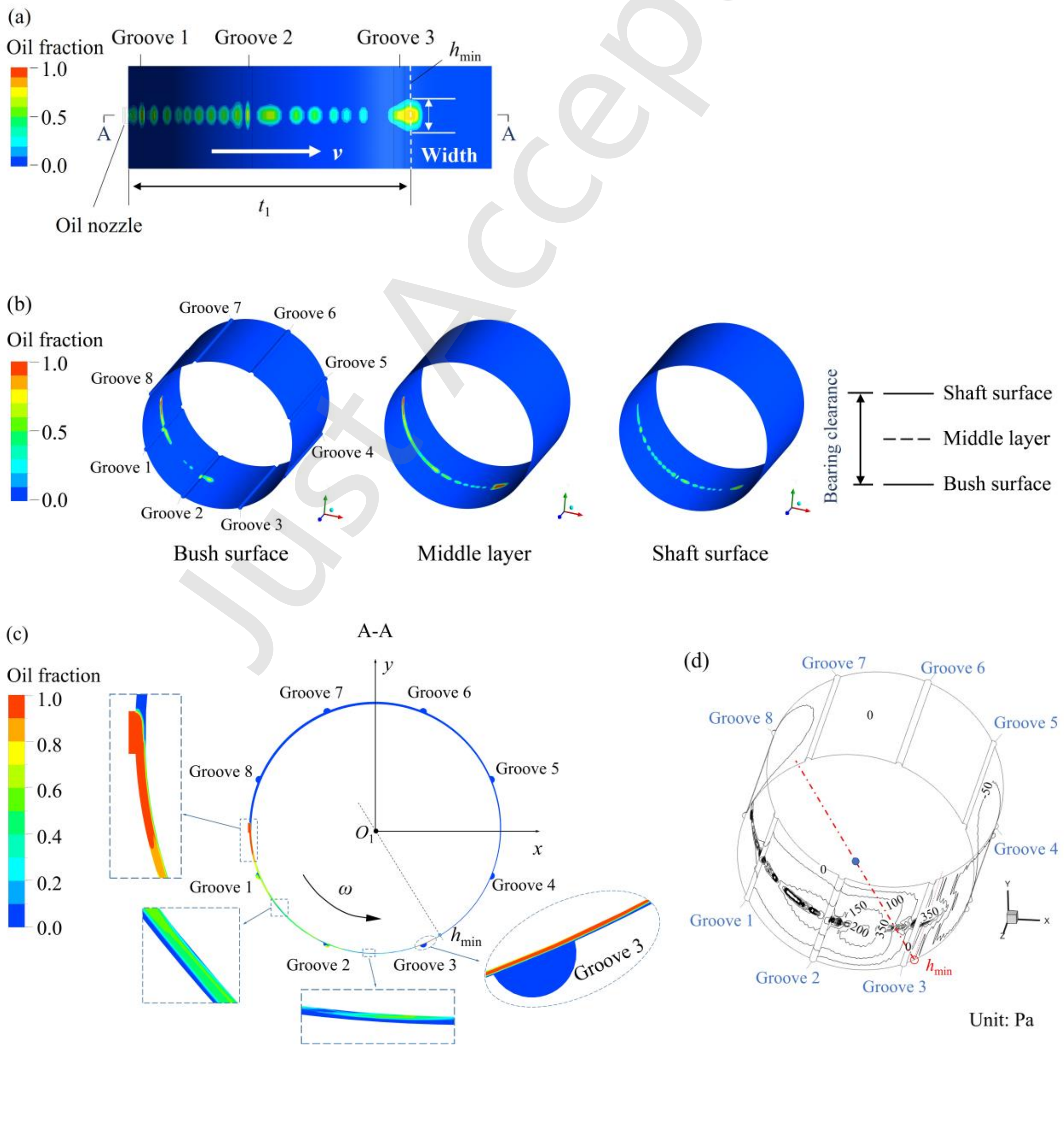

Fig. 11 Simulation of the oil transportation, ω = 100 r/min, t = 0.26 s; (a) Oil fraction on the shaft surface; (b) oil fraction in different layers; (c) oil fraction at the A-A cross section; (d) pressure distribution.

To gain more insight into the oil transportation oil diffraction on the surface of the bush and the shaft were calculated for various time instants, t = 0.65 s, 1.85 s and 3.05 s, as shown in Fig. 12. After the oil enters the contact region, leakage occurs when the oil film pressure is built. Notably the spread of the oil on the bush surface along the circumference direction is small, where oil mostly adheres to the region between Groove 1-Groove 3. This is attributed to the fact that the oil is injected just before Groove 1, and there is a divergency clearance after Groove 3 where cavitation can occur and the oil adhesion is broken. The axial oil spread between Groove 1 and Groove 2 is smaller than that between Groove 2 and Groove 3, which is due to that the oil enters a convergency clearance and consequently the oil spreads towards the two ends driven by the pressure gradient. Apparently, there is enough oil supply at this stage, inducing a COF drop, as shown in Fig. 5 and Fig. 7.

The distribution of oil on the shaft surface is different from that on the bush surface. Most of the oil stays near the central circumferential line. The adhesion of oil on the shaft surface contributes to the oil supply in the load-bearing area, which is also linked to the COF. The simulation results depicting pressure distribution under various rotation speeds are presented in Fig. 13. Time-varying nature of the oil in the contact zone causes the pressure distribution to also be time-varying.

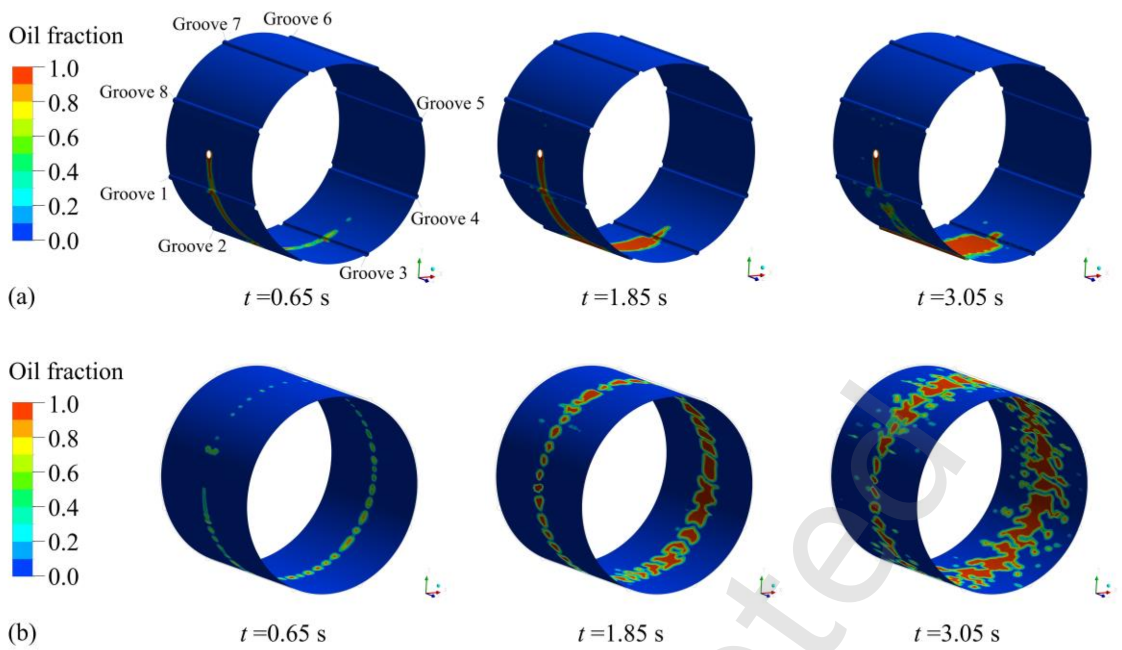

Fig. 12 Oil distribution (ω=100 r/min): (a) On the bush surface; (b) on the shaft surface.

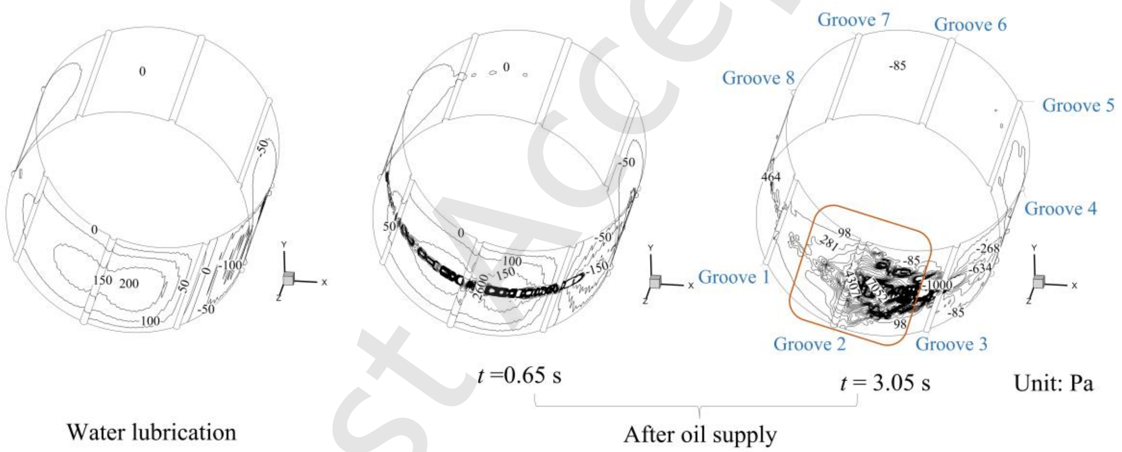

Fig. 13 Pressure distribution on the bush surface (ω=100 r/min).

Oil is driven by the pressure gradient along the axial direction and leakage occurs at both bearing ends. During the test, large leakage of oil lasts for several tens of seconds or even longer after the initiation of oil supply. Most of the oil stays in the convergence, which cannot pass through the minimum clearance or adhered to the bearing surface in a short time, so there is significant amount of side leakage. After the oil supply is stopped for a period of time, the remaining oil stays relatively stable and the mass flow of side leakage gradually reduce. However due to the existence of the pressure gradient in the convergence area, the oil will still migrate slowly to the side and cause leakage until all the oil is thoroughly consumed. When oil leakage is very small the COF becomes almost stable. This also implies that only a small volume of oil can actually contribute to stable lubrication.

In the CFD simulation, as an example, the oil leakage at the face of Outlet 1 (one of the outlets as shown in Fig. 4(b)) was monitored between 4 s and 9 s at 100 r/min. In the velocity field at the face of Outlet 1, the velocity pointing from the inside of the bearing toward the outlet is predominantly located in the convergence gap area, which indicates that most of the leakage occurs at the convergence gap area, as shown in Fig. 14(a). In Fig. 14(a), negative values represent fluid flowing out of the bearing, and positive values represent fluid flowing into the bearing. The leakage in the divergence gap area is small, which is consistent with the oil leakage in non-groove bearings [47]. The leakage primarily occurs in the non-groove area, covering 78.3% of the total leakage and denoted as Oths in Fig. 14(b). The leakage at the grooves accounts for 21.7% of the total leakage. Groove 2, Groove 1 and Groove 8 are the main regions where oil leakage occurs, and they are in the convergence gap area. Groove 2 accounts for 93.5% of the total groove leakage due to its larger pressure gradient, as depicted in Fig. 13. Considering Groove 2 as an example, it is observed that the axial velocity of the water phase is higher, while that of the oil phase is lower. This is attributed to the wall adhesion and higher viscosity of the oil, which act as resistance impeding the axial flow of the oil. Fig. 14(d) shows the oil fraction at different oil layers at t = 6 s. The oil mainly adheres to the rotating shaft surface, and oil distribution and leakage may vary at different layers. Additionally, the oil starts to leak during the oil supply period, signifying that an excessive oil supply would result in wastage of oil. Hence, it is essential to design appropriate oil supply parameters in practical applications. The side leakage of oil in the bearing clearance in water is the result of fluid mechanics and interface effect and the resistance terms of the momentum equation can be used to purposefully minimize oil leakage. Moreover the oil flow in the grooves is lower than that in the mainstream, and the accumulated oil within the grooves will be gradually released, enhancing assistant lubrication for the contact area. This suggests that the oil storage in the grooves may effectively extend the time of the assistant lubrication.

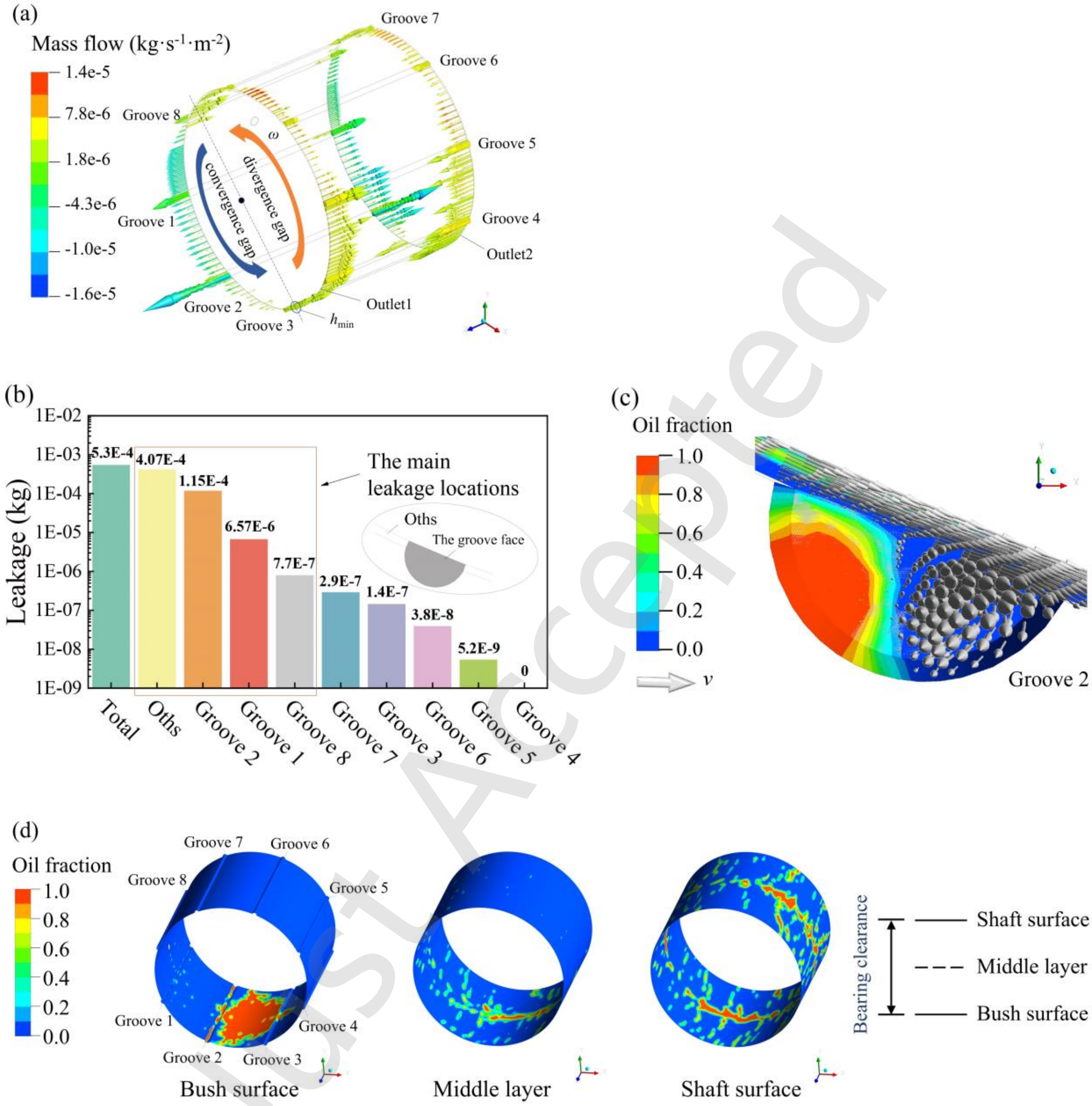

Fig. 14 Leakage at Outlet 1 face: (a) Fluid (water and oil) flow along the axial direction and mass flow of the slide at t = 6 s; (b) total oil leakage and leakage at each position at Outlet 1 face; (c) oil fraction and velocity field at Groove 2 at t = 6 s; (d) oil fraction in different layers at t = 6 s.

As the leakage decreases, low COF also tends to stabilize. Fortunately this low stable COF can last for a pretty long time, which is beneficial to avoiding risk from short-time sever working conditions. However the friction will increase eventually as the oil has been used up by side leakage and water wash. Evidently it is preferred to obtain low friction for a long time when this small-quantity oil assistance is used. Fig. 15 presents calculated oil leakage rate versus time at Outlet 1, and the shaft speed is 100 r/min. As stated above, the leakage rate increases first with the oil supply and then decrease gradually after the oil supply. In Fig. 15, it is interesting to put the measured coefficient vs. time (Fig. 5(a), 100 r/min) and to find that the unstable friction is in the period of high unsteady oil leakage rate, and the stable low COF is very correlated to the small stable leakage rate.

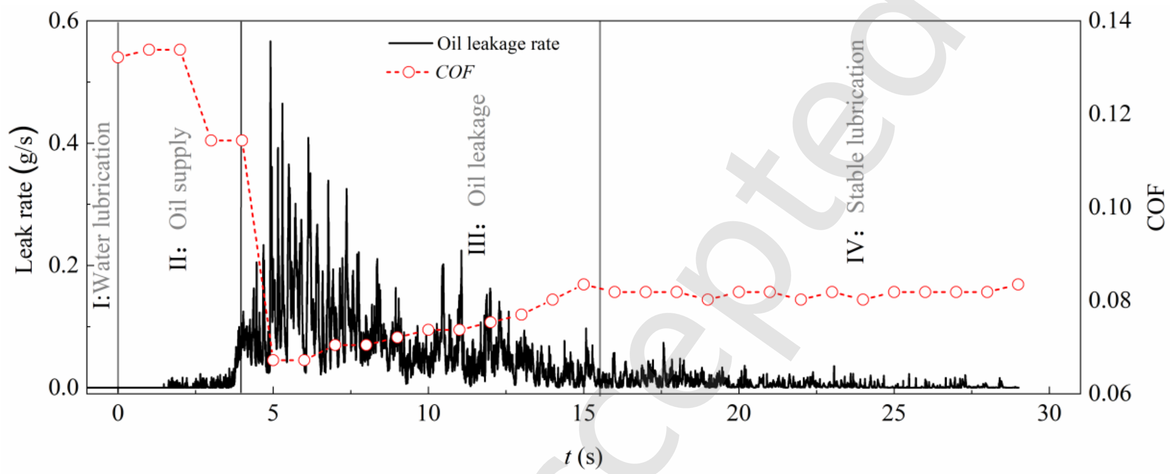

Fig. 15 Calculated oil leakage rate vs. time at Outlet 1, shaft speed = 100 r/min.

At 0.5 MPa and 300 r/min in test, the low COF time after oil supply is usually no more than 40 min, then COF will gradually increase and approach the value of water lubrication. The test results indicate that intermittent oil supplies can prolong the time of the stable lubrication, as depicted in Fig. 16(a). The COFs under various oil supply time intervals (5 min, 15 min and 30 min) during the assistant lubrication period are similar. Nevertheless, compared to the 30-minute oil supply interval, the 5-minute oil supply interval results in more fluctuations in COF. Perhaps there is still enough oil in the bearing clearance for oil supply at 5-minute interval, and at that time oil supply will lead to the increase in traction force and fluctuations in COF. A further 3-hour wear test was conducted, and the line wear rate (maximum wear depth of bush in radial direction) was 53 μm/h with pure water lubrication. Intermittent oil supply into the bearing can reduce the bush line wear rate by more than 80%. The line wear rates under various time intervals of oil supply are also similar as shown in Fig.

16(b). This indicates that excessively frequent oil supply will not yield more friction and wear reduction. In Fig. 16, the supply rate of silicone oil each time is 0.5 mL/s, and each supply lasts for 4 s. In practice, it is appropriate to accurately control the time interval of oil injection by monitoring the changes of the COF or other parameters.

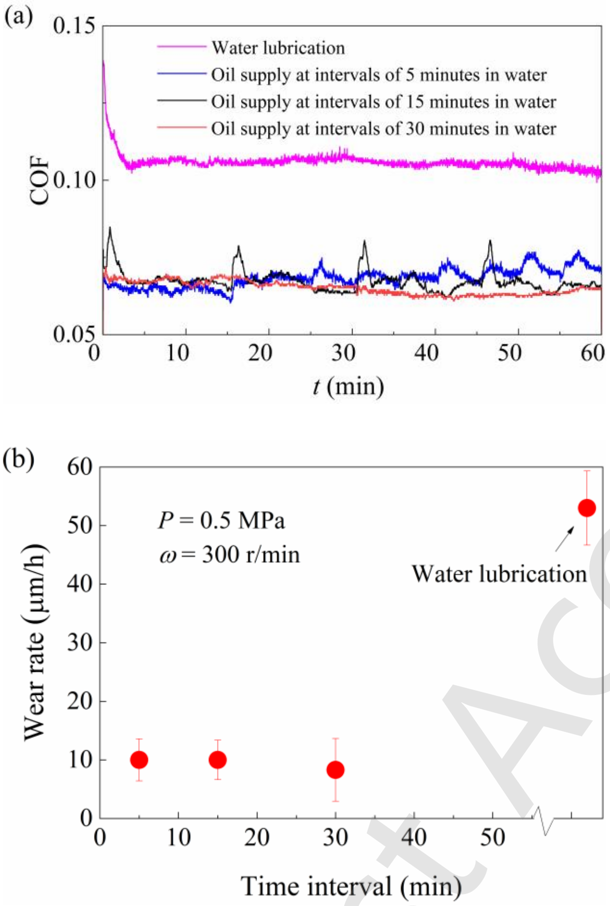

Fig. 16 Friction and wear under intermittent oil supply, P = 0.5 MPa, ω = 300 r/min: (a) COF with pure water and intermittent oil supply; (b) line wear rate at various time intervals.

When the quantity of oil is insufficient to provide effective lubrication, the COF becomes unstable and increases, and the oil-assisted water lubrication in the contact area gradually returns to pure water lubrication. In the CFD simulation, it can be represented as both the oil volume fraction in the clearance and the leakage rate approaching zero.

In the future, if some intelligent control methods are combined to monitor the increase in the COF of water-lubricated bearings, start the oil supply, and judge the oil supply interval when the ship is at low speed or subjected to load impacts such as ocean currents, it may have accurately reduced friction and significantly extend the life of the bearings.

4 Conclusions

Bench tests with an eight-groove rubber bearing have been conducted to investigate water lubrication assisted by a small quantity of silicone oil, demonstrating significant friction reduction under various specific pressures and lower shaft rotational speeds. By the CFD simulation, the transportation/diffusion of silicone oil in the water-lubricated rubber bearing was analyzed. The results can be summarized as follows:

(1) Supply of a small quantity of silicone oil in the bearing underwater can markedly reduce friction. The maximum COF reduction ratio can reach up to 73.8%, and the oil can remain in the open bearing clearance for a pretty long period. Under some working conditions, water lubrication assisted by a small quantity of silicone oil can attain a lower COF than that by either pure water or pure oil.

(2) Based on Stribeck-curve a simple approach to roughly predict COF reduction ratio with assistance of oil was presented assuming that apparent viscosity is similar after a small quantity of oil is supplied, which has been validated by the experimental data.

(3) CFD simulation showed that oil side leakage could last a few tens of seconds after oil supply. Furthermore, oil leakage predominantly occurs in the gap convergence area. The leakage of the water phase is higher than that of the oil phase, which is attributed to the wall adhesion and higher viscosity of the oil.

(4) Low COF can remain relatively stable for a long time. Intermittent oil supply can prolong the duration of low friction. In comparison to pure water lubrication, the line wear rate with multiple intermittent active oil supplies can be reduced by 84.3%. Frequent oil supply does not significantly increase the extent of friction and wear reduction ratio.

Limitations

(1) The CFD simulation employs a fixed film thickness method in this work. The CFD work does not delve into extensive quantitative research, instead, it focused on discussing typical characteristics.

(2) The test bearing has a relatively small length-to-diameter ratio, and environmentally friendly oil is not utilized.

(3) The influence of water axial flow in the bearing has not been considered.

Acknowledgements

This work is supported by National Natural Science Foundation of China (No. 52175173 & No. 52205200).

Declaration of competing interest

The authors have no competing interests to declare that are relevant to the content of this article.

References

[1] Wu Z M, Guo Z W, Yuan C Q. Insight into the influence of the anatomical properties of wood on the tribological properties. *J Clean Prod* **330**: 129800 (2022)

[2] Liu S T, Dong C L, Yuan C Q, Bai X Q. Friction reduction behavior of oil-infused natural wood[J]. *Friction* **10**(11): 1824-1837 (2022)

[3] Smith E H. On the design and lubrication of water-lubricated, rubber, cutlass bearings operating in the soft EHL regime. *Lubricants* **8**(7): 75 (2020)

[4] Wang H J, Liu Z L, Zou L, Yang J. Influence of both friction and wear on the vibration of marine water lubricated rubber bearing. *Wear* **376**: 920-930 (2017)

[5] Dong C L, Yuan C Q, Bai X Q, Yan X P. Study on wear behaviour and wear model of nitrile butadiene rubber under water lubricated conditions. *RSC Adv* **4**(36): 19034-19042 (2014)

[6] Huang J, Zhou X C, Wang J, Tang X W. Influence of temperature on friction of polymeric materials in water. *Wear* **426**: 868-876 (2019)

[7] Ning C X, Hu F, Ouyang W, Yan X P, Xu D L. Wear monitoring method of water-lubricated polymer thrust bearing based on ultrasonic reflection coefficient amplitude spectrum. *Friction* **11**(5): 685-703 (2023)

[8] Yu C Y, Ju P F, Wan H Q, Chen L. Designing a PAI/PTFE coating with enhanced high-temperature tribological properties by S8-POSS: solid-liquid dual lubrication. *Prog Org Coat* **145**: 105667 (2020)

[9] Liu X S, Zhou X C, Yang C Z, Huang J. Effect of interfacial interaction between Nano-SiO2 and NBR on tribological properties of NBR water-lubricated bearings. *Wear* **490**: 204191 (2022)

[10] Ren Y L, Zhang L, Xie G X, Li Z B, Chen H. A review on tribology of polymer composite coatings. *Friction* **9**(3): 429-470 (2021)

[11] Kuang F M, Zhou X C, Huang J, Zhou X R, Wang J. Tribological properties of nitrile rubber/UHMWPE/Nano-MoS2 water-lubricated bearing material under low speed and heavy duty. *J Tribol-T ASME* **140**(6): 061301 (2018)

[12] Wu Z M, Guo Z W, Yuan C Q, Huang Q R, Wang C, Zhao H Y. Lignum vitae wood-derived composites for high lubricating performance. *J Clean Prod* **406**: 137086 (2023)

[13] Yan Z M, Zhou X C, Qin H L, Niu W Y, Wang H, Liu K, Tang Y M. Study on tribological and vibration performance of a new UHMWPE/graphite/NBR water lubricated bearing material. *Wear* **332**: 872-878 (2015)

[14] Zhang W, Chen X Y, Yamashita S, Kubota M, Kita H. B_4C–SiC Ceramics with Interfacial Nanorelief Morphologies and Low Underwater Friction and Wear. *ACS Appl Nano Mater* **4**(3): 3159-3166 (2021)

[15] Zhang Y, Jiao J G, Chen H, Gao K, Ren Y L. Degradation induced superlubricity on the rough surface of black phosphorus composite. *Chem Eng J* **490**: 151507 (2024)

[16] Zhou G W, Wang J X, Han Y F, Li J Y. Study on the stiffness and damping coefficients of water-lubricated rubber bearings with multiple grooves. *P I Mech Eng J-J Eng* **230**(3): 323-335 (2016)

[17] Mallya R, Shenoy S B, Pai R. Static characteristics of misaligned multiple axial groove water-lubricated bearing in the turbulent regime. *P I Mech Eng J-J Eng* **231**(3): 385-398 (2017)

[18] Cai J L, Han Y F, Xiang G, Wang C, Chen S A. Influence of the mass conservation cavitation boundary on the tribo-dynamic responses of the micro-groove water-lubricated bearing. *Surf Topogr-Metrol* **10**(4): 045011. (2022)

[19] Brunetière N, Rouillon M. Fluid flow regime transition in water lubricated spiral grooved face seals. *Tribol Int* **153**: 106605 (2021)

[20] Wang N, Wang M W, YANG F. Multi-parameters fluidsolid coupling analysis on water-lubricated rubber bearings with eight grooves. *Bearing* **8**: 36-43 (2018)

[21] Gong J Y, Jin Y, Liu Z L, Jiang H. Study on influencing factors of lubrication performance of water-lubricated micro-groove bearing. *Tribol Int* **129**: 390-397 (2019)

[22] Li X F, Guo Z W, Huang Q R. Application of bionic tribology in water-lubricated bearing: a review. *J Bionic Eng* **19**(4): 902-934 (2022)

[23] Ramesh A, Akram W, Mishra S P, Cannon A. Friction characteristics of microtextured surfaces under mixed and hydrodynamic lubrication. *Tribol Int* **57**: 170-176 (2013)

[24] Huang X, Xu G, Jiang S Y. Study on rotor-bearing dynamic performance of a novel motorized spindle supported by water-lubricated hydrodynamic spiral grooved bearings. *Tribol Trans* **67**(4): 831-845 (2024)

[25] Ran H F, Dai P, Yan S P, Wang F T, Yao X J, Wang J P. Flow mechanisms and lubrication performance of water-lubricated thrust bearings with herringbone grooves. *Lubricants* **10**(8): 182 (2022)

[26] Wang N, Wang M W, Yang F. Multi-parameters fluid-solid coupling analysis on water-lubricated rubber bearings with eight grooves. *Bearing* **8**: 36-43 (2018)

[27] Zhou G W, Li R P, Liao D X, Yang W Y, Zhong P. Lubrication structure design of water lubricated rubber thrust bearing with spiral groove for shaftless rim driven thruster. *Tribol Int* **178**: 108098 (2023)

[28] Huang X, Zhang S W. Enhancing lubrication performance of fluid film journal bearings using combined effects of herringbone groove and porous bush. *Tribol Lett* **73**(1): 24 (2025)

[29] Litwin W. Experimental research on water lubricated three layer sliding bearing with lubrication grooves in the upper part of the bush and its comparison with a rubber bearing. *Tribol Int* **82**: 153-161 (2015)

[30] Xie Z L, Jiao J, Yang K, Zhang H. A state-of-art review on the water-lubricated bearing. *Tribol Int* **180**: 108276 (2023)

[31] Chen L, Qian L M. Role of interfacial water in adhesion, friction, and wear—A critical review. *Friction* **9**(1): 1-28 (2021)

[32] Zhang Z, Ouyang W, Liang X X, Yan X P. Review of the evolution and prevention of friction, wear, and noise for water-lubricated bearings used in ships. *Friction* **12**(1): 1-38 (2024)

[33] Guo C, Ye L, Weng K. Review of theory and experiment for underwater propulsion. In: 2023 International Conference on Marine Equipment & Technology and Sustainable Development, Singapore, 2023: 727-752

[34] Liu Q L, Ouyang W, Li R Q, Jin Y, He T. Experimental research on lubrication and vibration characteristics of water-lubricated stern bearing for underwater vehicles under extreme working conditions. *Wear* **523**: 204778 (2023)

[35] Li R Q, Ouyang W, Liu Q L, Jin Y, Yang J. Dynamic bearing characteristics of the ship stern shaft-bearing system with wave impact. *Ocean Eng* **312**: 119020 (2024)

[36] Yang T Y, Xiang G, Wang C, Wang L W, Jia H, Wang J X. Investigation on the transient asperity contact behaviours of water-lubricated bearing under start-stop cycle. *Int J Surf Sci Eng* **19**(1): 76-94 (2025)

[37] Wang B, Ouyang W, Wang S T, Sheng C X. Load carrying capacity enhancing design and lubrication investigation of the magnetic-water double suspension elastic support thrust bearing. *Lubricants* **11**(9): 401 (2023)

[38] Li R, Zhang X R, Yang P A, Han Y F. Magnetic-controlled friction behavior of a water-lubricated magnetorheological rubber bearing under boundary lubrication. *Tribol Int* **194**: 109499 (2024)

[39] Quinci F, Litwin W, Wodtke M. A comparative performance assessment of a hydrodynamic journal bearing lubricated with oil and magnetorheological fluid. *Tribol Int* **162**: 107143 (2021)

[40] Xiong W T, Shu X, Cheng S Y, Li X L, Zhang C H. Tribological performances of polytetrafluoroethylene/kevlar fabric liner reinforced by oil-containing microcapsules. *Tribol Int* **191**: 109119 (2024)

[41] Zhang Y, Chen H, Gao K, Li Y Z, Jiao J G, Ren Y L, Yu C C, Zhou G, Zhang L, Luo J B, Xie G X. Superlubricity Microcapsules. *ACS Appl Mater Interfaces* **17**(9): 14634-14644 (2025)

[42] Yang M M, Zhu X T, Ren G N, Men X H, Guo F, Li P L, Zhang Z Z. Tribological behaviors of polyurethane composite coatings filled with ionic liquid core/silica gel shell microcapsules. *Tribol Lett* **58**(1): 9 (2015)

[43] Li H Y, Wang Q, Wang H Y, Cui Y X. Fabrication of thermally stable polysulfone microcapsules containing [EMIm][NTf2] ionic liquid for enhancement of in situ self-lubrication effect of epoxy. *Macromol Mater Eng* **301**(12): 1473-1481 (2016)

[44] Guo Z W, Dong S K, Yang Z X. Tribological properties of aramid fiber-microcapsule modified ultra-high molecular weight polyethylene composites for water lubrication. *J Mater Eng Perform* **31**(7): 6000-6008 (2022)

[45] Zhang X H, Yu T, Guo F, Liang P. Analysis of the influence of small quantity secondary lubricant on water lubrication. *Tribol Int* **159**: 106998 (2021)

[46] Yu T, Zhang X H, Guo F. Enhancing water lubrication by secondary assistant lubricant in small quantity. *Tribology* **42**(2): 358-365 (2022)

[47] Liang Q C, Liang P, Guo F. Analysis of flow diffusion of secondary lubricant in water-lubricated bearings. *Phys Fluids* **35**(10) (2023)

Author biography

Tao YU. He now is a Ph.D. candidate in school of mechanical and automotive engineering, Qingdao University of Technology. His main research is water lubrication, aiming at reducing the friction and wear of water lubricated bearings through experiments and computational fluid dynamics (CFD) simulations.

Feng GUO. He got his Ph.D. from the City University of Hong Kong in Nov. 2003. He now serves as the dean of Yantai Automotive Engineering Professional College. He is a Taishan Scholar Chair Professor in Qingdao University of Technology. His main work is concentrated on fundamental research in tribology.